Electrochimica Acta 53 (2008) 5587–5596

Contents lists available at ScienceDirect

Electrochimica Acta

journal homepage: www.elsevier.com/locate/electacta

Electrochemical kinetics and X-ray absorption spectroscopy investigations of select chalcogenide electrocatalysts for oxygen reduction reaction applications

Joseph M. Ziegelbauer[a,1], Vivek S. Murthi[a,2], Cormac O'Laoire[a], Andrea F. Gullá[b], Sanjeev Mukerjee[a,*]

[a] Northeastern University, Department of Chemistry and Chemical Biology, Boston, MA 02115, USA
[b] De Nora R&D Division, 625 East Street, Fairport Harbor, OH 44077, USA

ARTICLE INFO

Article history:
Received 7 November 2007
Received in revised form 20 February 2008
Accepted 21 February 2008
Available online 4 March 2008

Keywords:
X-ray absorption spectroscopy
Activation energy
Chalcogenides
Rhodium sulfide
Ruthenium sulfide

ABSTRACT

Transition metal-based chalcogenide electrocatalysts exhibit a promising level of performance for oxygen reduction reaction applications while offering significant economic benefits over the state of the art Pt/C systems. The most active materials are based on Ru_xSe_y clusters, but the toxicity of selenium will most likely limit their embrace by the marketplace. Sulfur-based analogues do not suffer from toxicity issues, but suffer from substantially less activity and stability than their selenium brethren. The structure/property relationships that result in these properties are not understood due to ambiguities regarding the specific morphologies of Ru_xS_y-based chalcogenides. To clarify these properties, an electrochemical kinetics study was interpreted in light of extensive X-ray diffraction, scanning electron microscopy, and *in situ* X-ray absorption spectroscopy evaluations. The performance characteristics of ternary $M_xRu_yS_z$/C (M = Mo, Rh, or Re) chalcogenide electrocatalysts synthesized by the now-standard low-temperature nonaqueous (NA) route are compared to commercially available (De Nora) Rh- and Ru-based systems. Interpretation of performance differences is made in regards to bulk and surface properties of these systems. In particular, the overall trends of the measured activation energies in respect to increasing overpotential and the gross energy values can be explained in regards to these differences.

1. Introduction

The arguably largest impediment against the adoption of polymer exchange membrane or direct methanol fuel cells (PEMFC and DMFCs, respectively) is an economical constraint, for they still rely upon expensive noble metal (Pt-based) electrocatalysts to achieve their performance levels. While state of the art Pt-based electrocatalysts exhibit good kinetics and activity towards oxygen reduction reaction (ORR), Pt remains just as selective towards various contaminants. The result of fuel/oxidizer feeds contaminated with halide anions, ubiquitous organics, and/or methanol crossover results in inherent side reactions that reduce the efficiency of the full $4e^-$ ORR pathway, and often leads to increased peroxide production via promotion of the simultaneous $2e^-$ pathway [1,2]. Decades of study regarding Pt-based systems [3,4] have resulted in significant mitigation of these performance-robbing effects. For example, Pt–Ru systems are now generally accepted as the state-of-the-art anode materials in relation to their CO tolerance [3,4]. On the cathode side, Pt–M alloys (M = Co, Ni, etc.) have been shown to mitigate the unwanted surface poisoning effects of OH adsorption versus molecular oxygen adsorption through a combination of electronic and bifunctional mechanisms [5–7]. Overall, while these advances have served to improve the performance of Pt-based PEM/DMFCs by several fold, the scarcity and cost (1200 $USD per troy ounce, ~31 g) [8] of Pt remains a serious disadvantage.

As a result, a large variety of alternative materials have been investigated for ORR applications. Key to the realization of low temperature PEMFCs is overcoming the expense of Pt-based electrocatalysts, and the obvious route is to substitute less expensive metals. The literature is full of examples of more economical transition metal-based catalysts for ORR applications [9,10]. However, while these materials have shown a promising level of activity towards ORR (in addition to well-established levels of methanol tolerance) [10], their applicability is stymied by less than desirable corrosion resistance and longevity. Resolution of these issues

* Corresponding author at: Northeastern University, Department of Chemistry and Chemical Biology, 360 Huntington Ave, Boston, MA 02115, USA.
Tel.: +1 617 373 2382; fax: +1 617 373 8949.
E-mail address: s.mukerjee@neu.edu (S. Mukerjee).
[1] Current address: General Motors Research and Development Center, M/C: 480-102-000, 30500 Mound Road, Warren, MI 48090, USA.
[2] Current address: NIST Center for Neutron Research, 100 Bureau Drive, MS 6102, Building 235, Room E130-3, Gaithersburg, MD 20899, USA.

0013-4686/$ – see front matter © 2008 Elsevier Ltd. All rights reserved.
doi:10.1016/j.electacta.2008.02.091

is made even more difficult by inconsistencies in their synthesis, preparation, and evaluation from one research group to another. Of these alternative systems, one of the most-studied and promising are the chalcogenide electrocatalysts [11].

Initially investigated for applications in solar cells, chevrel-phase sulfides were reported as exhibiting appreciable activity for ORR in 1986 [12]. Over the following years [11,13,14], it was discovered that the activity of the chalcogenide materials was further improved by the addition of various transition metals (e.g. Mo, Rh, Re, etc.) to the Ru_xS_y or Ru_xSe_y matrices [11,15–17]. In addition to numerous electrochemical studies, analysis of small angle X-ray scattering [18] and various X-ray absorption spectroscopy (XAS) studies [19–22] have provided the following overview:

1. The now-standard "nonaqueous" synthetic process [11,23] results in discrete metal nanoparticles (typically Ru) with a surface coverage of the respective chalcogen [11,24], and these surface chalcogen deposits serve to stabilize ruthenium against corrosion.
2. Transition metal "additives" in ternary ($M_xRu_yS_z$ or $M_xRu_ySe_z$) clusters are not present within (i.e. interstitially) the resulting Ru nanoparticles [11,21,22].
3. Overall the Ru_xSe_y-based materials exhibit higher activity than their sulfur-based analogues [11,21,22,24,25].
4. Regardless of the choice of chalcogen (sulfur or selenium), the materials are essentially totally tolerant to methanol [10,11,15,16].

Although the selenium-based materials outperform their respective sulfur-based analogues, the toxicity of selenium renders the commercialization of these materials untenable. This leaves the sulfur-based materials as the only commercially viable option. Unfortunately, these types of catalysts do not approach the performance gains observed with the selenium materials [11]. In addition there remain serious questions regarding the long-term stability of these materials [24] as the sulfur-based catalysts exhibit an appreciably shorter life span than the selenium-based analogues. A carbon-supported Rh_xS_y chalcogenide electrocatalyst developed by Industrie De Nora, S.p.A. alleviates the toxicity and stability issues by avoiding both selenium and the nonaqueous synthetic route completely. This material is synthesized via a sulfur ion-free process [26]; a low-temperature aqueous method that does not require elemental sulfur as a precursor. The resulting electrocatalyst is comprised of a balanced phase mixture [27] of $Rh_{17}S_{15}$, Rh_3S_4, and Rh_2S_3 with the Rh_3S_4 phase acting as the active phase [28,29]. The material is inherently stable as evidenced by its activity for ORR as an oxygen depolarized cathode (ODC) for HCl electrolysis applications [30]. Despite the economical issues arising from the extreme rarity and expense of rhodium metal [8], a recent study has shown that the overall metal loading of the electrocatalyst can be significantly reduced without a loss in activity [31]. To date, this material remains the only commercially available chalcogenide electrocatalyst sold for ORR applications.

ORR on metallic surfaces is generally described by a mechanism first proposed by Damjanovic et al. [1] for Pt-based materials. Full ORR is comprised of a $4e^-$ reduction pathway resulting in the conversion of oxygen to water with a ubiquitous $2e^-$ pathway that results in the PEM-damaging production of hydrogen peroxide [2]. The fact that Pt (an fcc metal with the $Fm\bar{3}m$ space group) is easily separated into homogeneous single crystal planes has greatly assisted in elucidating the ORR process [32]. As technology further developed, various spectroscopic techniques [33–39] were performed in conjunction with electrochemical studies to identify the nature and chemistry of adsorption phenomena associated with ORR [32]. To a lesser extent, these studies have also been performed on ruthenium [40] and rhodium [41,42]. A novel analysis of *in situ* X-ray absorption spectroscopy (XAS) results provided the first spectroscopic observation of water activation on a chalcogenide electrocatalyst (De Nora's Rh_xS_y/C) [28,29]. However, nanoparticles of Ru_xS_y or Ru_xSe_y are far less understood, for the underlying structures of these materials do not lend themselves to single crystal studies.

In this report we address some of the deficiencies in describing the electrocatalytic activity of Ru-based sulfide chalcogenide electrocatalysts. Bulk properties of several catalyst varieties were probed with X-ray diffraction and standard SEM/EDX techniques. In an effort to clarify the short-range order characteristics, an extensive *in situ* XAS investigation was conducted. These structural characteristics are interpreted in conjunction with both standard electrochemical kinetic studies and activation energy measurements.

2. Experimental

2.1. Synthesis

The materials investigated in this work were synthesized via methods previously outlined in a prior publication [30]. Briefly, the $Mo_xRu_yS_z$/C, $Rh_xRu_yS_z$/C, $Re_xRu_yS_z$/C, and Rh_xS_y/C were synthesized from metal carbonyl precursors and elemental sulfur via the nonaqueous (NA) route first reported in detail by Solorza-Feria et al. [23] The Ru_xS_y/C material was created utilizing the "gas–solid" reaction (SS), which involved a high temperature thermal treatment of the chloride precursor under 1:1 H_2S:N_2. The commercially available Rh_xS_y/C catalyst from De Nora was synthesized by the patented aqueous "sulfur ion-free" process (SF) [43]. All catalysts were synthesized such that they were 30 wt% *metal* loading on Vulcan XC-72 carbon black (Cabot Corporation). The 30 wt% Pt/C standard electrocatalyst was purchased from E-TEK, Inc. (now "BASF Fuel Cell Inc.", Somerset, NJ), and used as-received.

2.2. Morphology

2.2.1. X-ray diffraction and SEM/EDX

The X-ray diffraction and SEM/EDX studies have been discussed in a recent publication [30]. Briefly, powder X-ray diffraction studies were performed in the laboratory on a Rigaku D/MAX-2200 series instrument equipped with a Cu Kα X-ray source (1.5405 Å). For the highly amorphous (NA) chalcogenide electrocatalysts, high intensity synchrotron radiation (0.9212 Å, beamline X-7B, The National Synchrotron Light Source, Brookhaven National Labs, Upton, NY) was utilized. SEM/EDX measurements were performed on a Hitachi S-4800 SEM/EDX. The relative at.% ratios of metal(s):sulfur of the as-synthesized electrocatalysts were determined via EDX over three randomly selected areas at 5 and 20 keV.

2.2.2. X-ray absorption spectroscopy

All experiments were conducted at room temperature in an inert electrochemical cell (based on a previously reported design) [28,44] at beamlines X-11A and X-18B at the National Synchrotron Light Source (Brookhaven National Labs, Upton, NY). The 5-cm^2 working electrodes consisted of 95:5 (by mass) 30 wt% chalcogenide electrocatalyst:Nafion® hand painted onto commercially available LT1400W (BASF) gas diffusion layers. The total geometric loading of the cathodes (2.0–5.0 mg metal cm^{-2}) was chosen to give a transmission XAS absorption cross-section of at least 0.2. A Nafion® 112 membrane (DuPont) acted as the separator, and a thin Au wire (0.35 mm, 99.99%, Alfa Aesar) functioned as the counter electrode. Before assembling the cells with the respective cathode, the electrodes were vacuum-soaked in de-aerated electrolyte for 1 h, and then lightly rinsed with deionized water. The electrolytes utilized

in the XAS experiments were 1M trifluoromethanesulfonic acid (TFMSA, 3 M Corp.). TFMSA was chosen for its low anion adsorption effects [45], and was triply distilled to remove impurities [46,47]. All electrolytes were de-aerated by bubbling Argon for 20 min prior to introduction into the cell to remove any possible interference towards the water activation process. A sealed RHE, generated from 1 M TFMSA to eliminate junction potentials, served as the reference electrode. All potentials are reported in respect to RHE (0.00 V vs. H^+/H).

The catalysts were activated by scanning 3–5 times between the following potential windows: 0.02–0.85 V (Ru-based systems), or 0.02–1.1 V (Rh-based systems). The cells were potentiostatically controlled by an Autolab PGSTAT30 bipotentiostat/galvanostat (Eco Chemie, Brinkmann Instruments). Full Ru or Rh K edge (22117 and 23220 eV, respectively) extended X-ray absorption fine structure (EXAFS) scans were collected in 100 mV intervals from 0.30 V on the anodic sweeps. In the X-ray absorption near edge spectroscopy (XANES) region the scans were collected in 1.2 eV steps due to the large core hole lifetimes exhibited at the Rh and Ru K edges. All measurements were collected in the transmission mode in conjunction with a Ru powder or Rh foil residing in the reference channel to aid in energy calibration and alignment. All EXAFS analysis [48] was performed with the IFEFFIT Suite (Version 1.2.8, IFEFFIT Copyright 1997–2002, Matthew Newville, http://cars9.uchicago.edu/ifeffit/) [49]. In addition, single XANES scans at the Mo K, Rh K, and Re L_3 edges were performed on the $Mo_xRu_yS_z$/C, $Rh_xRu_yS_z$/C, and $Re_xRu_yS_z$/C electrocatalysts in order to determine the atomic ratios of the incorporated metals in an *in situ* operating environment.

2.3. Rotating ring disk electrode measurements

The RRDE experiment methodologies followed procedures described in detail in prior reports [6,28,50]. Briefly, inks of 30 wt% catalyst were prepared from 1:1 vol% deionized water (18.2 MQ, Millipore MilliQ) and 2-propanol (HPLC grade, Sigma–Aldrich) with a small amount of 5 wt% Nafion® solution (Aldrich). The ink was cast onto a polished 5 mm diameter (0.283 cm^2 geometric area) glassy carbon RRDE electrode (Pine Instrument Co.) previously polished to a mirror finish with 1 and 0.05 μm alumina slurries (Buehler). The final metal loading of all the studied catalysts was 14 $\mu g\,cm^{-2}$ (geometric), and the Nafion®:catalyst ratio was 1:50 (by mass) thus allowing for the neglect of additional diffusion effects [6,50]. Prior to the RRDE experiments, the materials were activated by scanning over the afore-mentioned electrochemical windows in de-aerated (N_2 bubbling) electrolyte. Because the Ru- and Rh-based electrocatalysts did not display a well-defined H^+/H adsorption/desorption region, all surface areas are reported in terms of geometric area as opposed to electrochemical surface area. Five full scans (20 mV s^{-1}) at each rotation rate (100, 400, 625, 900, 1225, 1600, and 2500 rpm) were collected in O_2-saturated (at least 20 min bubbling) 0.5 M H_2SO_4 and 0.5/1.0 M H_2SO_4/methanol controlled with a Pine Instruments (AFSAR) analytical rotator. While the effects of bisulfate anion adsorption on a large variety of electrocatalysts is well established [51–53], 0.5 M H_2SO_4 was chosen as the supporting electrolyte for the electrochemical measurements as it seems to have become the *de facto* standard for chalcogenide electrocatalysts [24,25,54–56]. Peroxide yields were obtained by holding the activated Au ring at 1.3 V and measuring the change in ring current in respect to the disk current. The collection efficiency of the ring ($N = 0.19$) was determined in 0.1 M NaOH + 10 mM $K_3Fe(CN)_6$ according to standard procedures [50,57,58]. Activation energies in 0.5 M H_2SO_4 were obtained by repeating the RRDE experiments at temperatures of 20, 30, 40, 50, and 60 °C utilizing a water-jacketed cell interfaced with an exacal® EX-300 temperature bath (NesLab Corp.). The temperature was controlled through a PTFE-coated K-type thermocouple (Omega, ±0.1 °C) placed in the electrolyte. Due to the high vapor pressure of methanol (16.9 kPa at 298 K vs. 3.16 kPa for water), in addition to the amount of time required to collect data at all of the temperatures, it was impossible to perform this experiment in the 0.5/1.0 M H_2SO_4/methanol electrolyte. At least three different trials were performed for each experiment to allow a proper determination of the experimental error.

3. Results and discussion

3.1. Morphology

3.1.1. X-ray diffraction and SEM

Graphs of the resultant XRD spectra are presented in Figs. 1 and 2. As an extensive analysis of these results has been

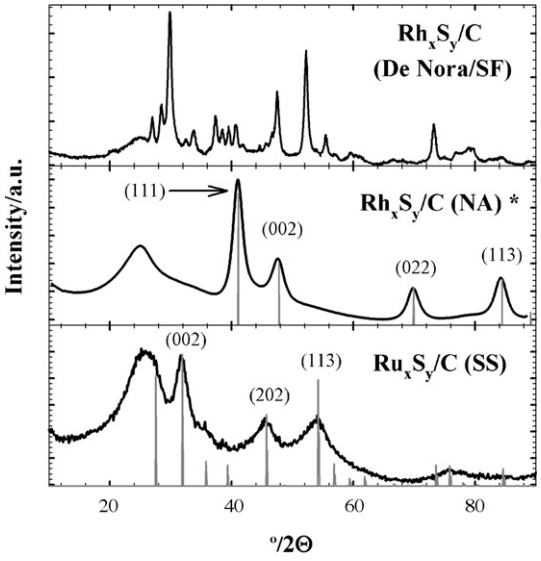

Fig. 1. X-ray powder diffraction spectra for the binary chalcogenide electrocatalysts described in the text. See Table 1 for determined elemental compositions. These spectra were originally published in Ref. [30].

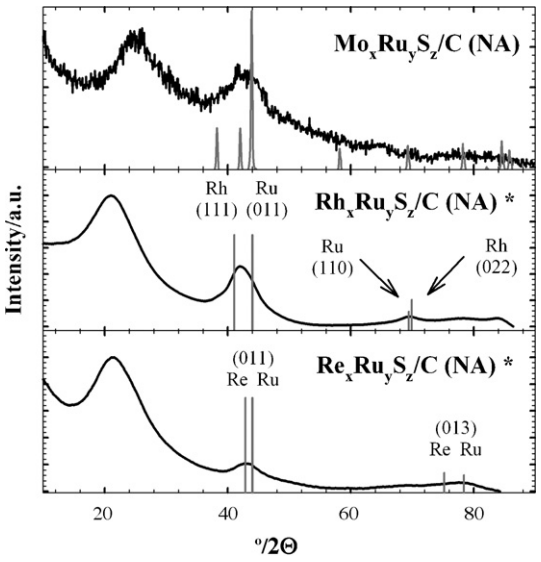

Fig. 2. X-ray powder diffraction spectra for the ternary chalcogenide electrocatalysts described in the text. See Table 1 for determined elemental compositions. All three spectra are indexed to P(6)3/mmc Ru (JCPDS no. 06-0663). These spectra were originally published in Ref. [30].

Table 1
Stoichiometry

Catalyst (30 wt%)	Target x:y:z (at.%)	As-synthesized x:y:z (at.%)[a,b]	Post-cycling x:y (at.%)[c]
Rh_xS_y/C (SF)	N/A	1.1:1	N/A
Rh_xS_y/C (NA)	1:1	1.1:1	N/A
$Mo_xRu_yS_z$/C (NA)	1:1.5:5	0.8:1.5:3.9	1:22
$Rh_xRu_yS_z$/C (NA)	1:1.5:5	1:1.5:5	1:12
$Re_xRu_yS_z$/C (NA)	1:1.5:5	0.8:1.5:4.4	1:24
Ru_xS_y/C (SS)	N/A	1:2.2	N/A

[a] EDX measurements, ±0.08.
[b] Previously published in Ref. [30].
[c] XAS (NSLS) edge height comparisons.

published in a prior report [30], the results will only be briefly summarized here. The differences in the SF- and NA-synthesized Rh_xS_y/C electrocatalysts (Fig. 1) were attributed to the differences in synthetic methodology. The SF method produces a balanced-phase mixture [27] of Rh_2S_3, Rh_3S_4, and $Rh_{17}S_{15}$ with the latter phase dominating the spectrum [28]. Further, the SF synthesis is followed by a high-temperature thermal treatment which results in a larger particle size. In contrast, the spectrum for the Rh_xS_y/C (NA) material (collected with high intensity synchrotron radiation) exhibits only the fingerprint of $Fm\bar{3}m$ rhodium metal (particle size 3.2 nm). Such a result was not unexpected, for it has been previously reported that the NA synthesis results in metallic Rh nanoparticles with a coating of the respective chalcogen [18,59]. Another example of the effect of the synthetic methodology on particle morphology was observed in the Ru_xS_y/C (SS) material (Fig. 1, bottom). As a result of the high temperature disproportionation of the chlorides with sulfur (from the $H_2S_{(g)}$ source) the material took on a pyrite-type ($Pa3$) structure. This can be contrasted to materials analogous in morphology to the Rh_xS_y/C (NA) material reported by other groups [11,15,18,24,59]. XRD studies of the three ternary $M_xRu_yS_z$/C (M = Mo, Rh, or Re) electrocatalysts (Fig. 2) revealed the expected morphologies for NA-synthesized materials. While the small particle sizes (~2.5 nm) and amorphous character of the materials contributed to the considerable difficulty in indexing the species, it was concluded that the materials consist of discrete M_xS_y and Ru_xS_y nanoparticles.

SEM/EDX studies were also performed in an effort to discern the mean aggregate sizes and as-synthesized stoichiometry of the materials (Table 1). The SF and SS synthetic methods resulted in larger aggregate sizes when compared to the NA materials. However, in contrast to the expectations arising from the XRD studies (Fig. 1), the Ru_xS_y/C (SS) material showed an elemental Ru:S at.% ratio of 1:2.2. This was attributed to the presence of non-laurite (RuS_{2-x}) phases or an excess of sulfur deposited during the disproportionation [30]. Another interesting result involved the stoichiometries of the $M_xRu_yS_z$ ternary chalcogenides. The target at.% compositions for M:Ru were 1.0:1.5, but only the $Rh_xRu_yS_z$/C material attained that ratio. The Mo and Re-containing varieties exhibited ratios of 0.8:1.5 suggesting that it is either: (1) much more difficult to incorporate Mo and Re into the $M_xRu_yS_z$-class of materials than Rh, or (2) the Mo and Re exist as discrete M_xS_y nanoscale clusters with a far lower stability to irreversible oxidation and dissolution in low pH environments [15,17].

3.1.2. X-ray absorption spectroscopy

3.1.2.1. XANES. The *in situ* (0.40 V) Rh K edge XAS absorption spectra for the Rh-based electrocatalysts are presented in Fig. 3. The main oscillatory features associated with fcc Rh are still visible in the Rh_xS_y/C (NA) electrocatalyst, but are considerably muted due to both the nanoscale- and sulfur-passivated nature of the Rh nanoparticles. Nonetheless, edge energy analysis (a quantitative equivalency of the oxidation state of the Rh absorber) [48,60] shows that the Rh in the Rh_xS_y/C (NA) electrocatalyst is identical to the Rh foil (oxidation state of 0). Akin to the Rh_xS_y/C (NA) spectrum, the

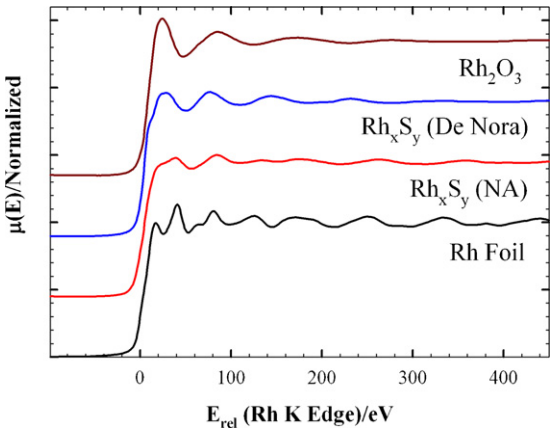

Fig. 3. *In situ* (0.40 V) Rh K edge (23220 eV) XANES.

Rh_xS_y/C (De Nora/SF) material is also considerably muted. However, the white line feature and position of the oscillations suggest that the De Nora material is not comprised of fcc Rh metal. In fact, the De Nora electrocatalyst exhibits a combination of features seen in both the Rh foil and Rh_2O_3 (*ex situ* standard) spectra. In particular the white line of the De Nora electrocatalyst is much larger than that observed for the Rh_xS_y/C (NA) material although it does not approach the magnitude of the Rh_2O_3 standard. According to the exhibited edge energy, the bulk Rh oxidation state in the De Nora electrocatalyst can be assigned as $Rh^{1.2+}$.

The analogous Ru K edge absorption spectra for the Ru-based electrocatalysts (Fig. 4) present a more complicated scenario. The overall spectra of all four chalcogenide electrocatalysts are muted indicating their nanoscale nature. Of the ternary electrocatalysts, only the $Rh_xRu_yS_z$ material is similar to the Ru foil standard in the oscillatory region. In contrast the white lines of the Mo- and

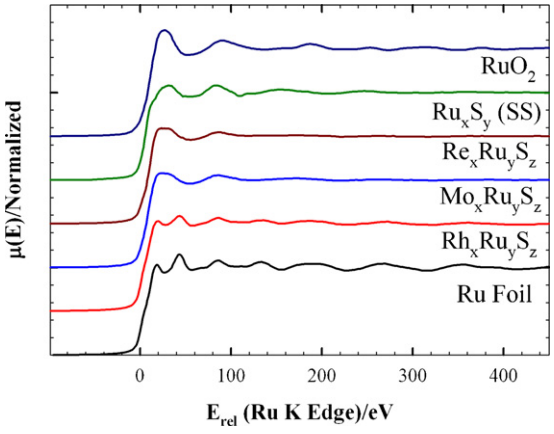

Fig. 4. *In situ* (0.40 V) Ru K edge (22117 eV) XANES.

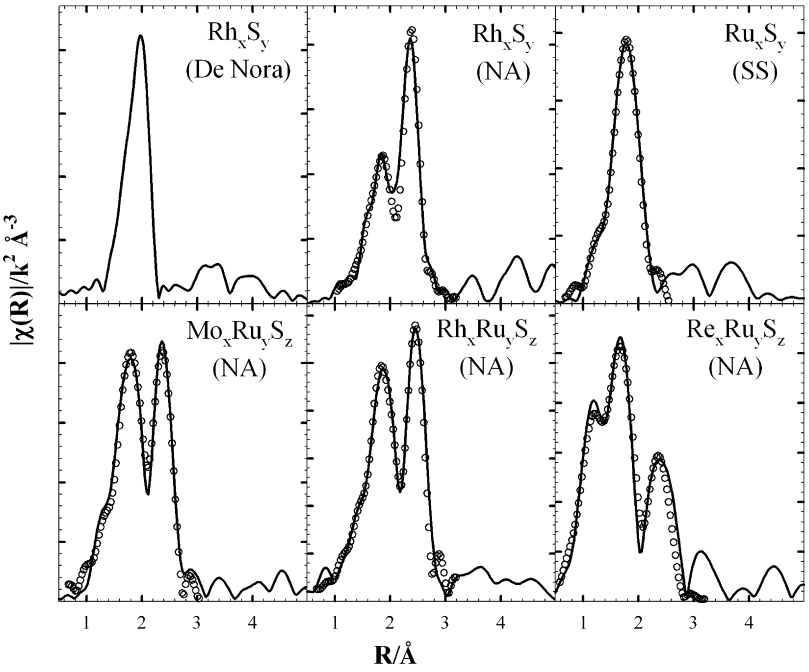

Fig. 5. Representative non-phase-corrected K edge (Ru or Rh) k^2-weighted *in situ* (0.40 V) EXAFS spectra of the chalcogenide electrocatalysts: experimental (—), first shell fits (○).

Re-based materials are suggestive of the *ex situ* RuO_2 standard while the oscillatory features are a mixture of those observed for the Ru foil and Ru_xS_y (SS) material. This is further reflected in the determined bulk oxidation states of the Mo- and Re-based ternaries, which show 1.2+ and 2.4+ Ru oxidation states, respectively. These values lay between the Ru(IV)O_2 and Ru^{0+} Ru foil standards. The Ru_xS_y (SS) electrocatalyst exhibits an edge energy indicating a bulk Ru oxidation state of ~2.5 (the RuO_2 standard gives 4+) in agreement with the EDX and XRD studies which suggested a non-stoichiometric Ru(II)S_2 pyrite. In addition, the white line and observable oscillatory features indicates that the SS material is not a RuO_2-type oxide. It can therefore be surmised that the Ru in the $Rh_xRu_yS_z$ material possesses a greater extent of metallic fcc Rh character than the Mo and Re-containing analogues (which exhibit features indicative of mixed metallic and oxidized Ru nanoparticles), and the Ru_xS_y/C (SS) electrocatalyst possesses the signature of pyrite.

3.1.2.2. EXAFS. Representative first shell (k^2-weighted) fitting results of 0.40 V *in situ* data for the electrocatalysts are presented in Fig. 5. The De Nora Rh_xS_y/C electrocatalyst, due to its mixed phase character, is too complex for this report, and is investigated in separate publications [28,29,61]. A high quality fit of the experimental data for the Rh_xS_y/C (NA) electrocatalyst was achieved by utilizing information from the XRD analysis in conjunction with standard models. While fcc Rh theoretically has a first shell N_{Rh} of 12, the values for the Rh_xS_y/C (NA) electrocatalyst was found to much lower (Table 2). This is indicative of the nanoscopic nature (3.2 nm grain

Table 2
EXAFS fit results

Catalyst	E (V)	M–M		M–S		M–O		E_0 (eV)	ΔR_{M-M} (Å)	χ^2 reduced
		N	R (Å)	N	R (Å)	N	R (Å)			
	0.54	8.5	2.664	2.5	2.298	–	–	−1.15	−0.025	153
Rh_xS_y (NA)[a]	0.70	8.5	2.666	2.5	2.293	–	–	−2.74	−0.023	134
	0.90	8.3	2.666	2.5	2.291	–	–	−2.24	−0.024	181
	0.40	3.4	2.684	1.6	2.285	0.1	1.877	−4.11	−0.062	43.2
$Mo_xRu_yS_z$[b]	0.60	3.4	2.686	1.7	2.278	0.1	1.879	−3.87	−0.075	42.4
	0.80	3.8	2.688	1.5	2.275	0.1	1.881	−2.96	−0.072	51.7
	0.40	4.2	2.709	2.7	2.311	0.2	1.901	3.68	−0.035	224
$Rh_xRu_yS_z$[b]	0.60	4.2	2.708	2.7	2.312	0.2	1.900	3.95	−0.035	147
	0.80	4.2	2.710	2.8	2.307	0.2	1.902	3.49	−0.040	133
	0.40	2.1	2.717	2.0	2.190	2.2	1.909	−36.1[c]	−0.158	30.1
$Re_xRu_yS_z$[b,c]	0.60	2.3	2.714	1.3	2.226	1.5	1.906	−24.4[c]	−0.121	65.9
	0.80	2.3	2.704	0.8	2.278	0.9	1.896	−11.3[c]	−0.069	54.2
Ru_xS_y (SS)[b]	N/A[d]	–	–	4.0	2.332	–	–	−1.12	−0.15	58.3

Error limits: $N \pm 20\%$, $R \pm 0.02$ Å.

[a] Fitting parameters for Rh: $S_0^2 = 0.921$ via FEFF, $\sigma^2 = 0.005$ Å^2.

[b] Fitting parameters for Ru: $S_0^2 = 0.901$ via FEFF, $\sigma^2 = 0.003$ Å^2.

[c] Inadequate fit due to heterogeneous nature. See text for details.

[d] *Ex situ* data.

size via XRD) of this material. Because of unavoidable instrument issues, it was impossible to collect *in situ* data for the Ru_xS_y/C (SS) electrocatalyst. Nonetheless, modeling of the Ru–S interaction from a pyrite (*Pa*3) RuS_2 model provided a fit (to an *ex situ* dataset) in excellent agreement with the XRD and EDX results.

The ternary chalcogenide electrocatalysts (Fig. 5, bottom) continue to exhibit trends suggested by the XANES analysis. The spectra and fits (Table 2) for the Rh- and Mo-based materials are very similar, and suggest that these catalysts are primarily composed of Ru nanoparticles with a surface layer of sulfur. It was found that Ru–M (M = Mo, Rh, or Re) did not contribute to the spectra at all. At all potentials, it was difficult to discern unique Ru–O interactions. This was attributed to several aspects of the collected data. First, the *in situ* data were collected in Ar-purged electrolyte thereby reducing the availability of dissolved molecular oxygen for adsorption onto the electrocatalyst surfaces. Further, the strength of S or O scattering on the electrocatalyst surface is similar. Finally, EXAFS is a bulk averaging spectroscopy, and is dominated by Ru–Ru interactions arising from within the Ru nanoparticles.

In contrast to the $Mo_xRu_yS_z$ and $Rh_xRu_yS_z$ electrocatalysts, the spectrum for the $Re_xRu_yS_z$ material is significantly different. While it was possible to separate the spectrum into Ru–Ru and Ru–X (X = low Z element) interactions based on the observed interatomic distances, the notable split of the low-R peak is unique. For the Mo- and Rh-based ternary electrocatalysts, this low-R peak was attributed to Ru–S interactions with contributions from Ru–O. The split in the Re-based ternary peak, however, suggests a heterogeneous mixture comprised of Ru–O and Ru–S interactions (interatomic distances at 2.0 and 2.35 Å, respectively). As the synthetic temperatures and conditions [23] for the NA electrocatalyst were too low to result in a pyrite-type RuS_2 structure, it is postulated that the material is comprised of mixture of discrete Ru oxides and sulfur-passivated Ru nanoparticles. This is in agreement with the XANES results. While methods such as Principle Component Analysis (PCA) could offer the necessary tools to fit this spectrum [62,63], it is unable to be applied in this particular case. Specifically, PCA requires a database of known standards. While RuO_2 and (pyrite) RuS_2 are readily available, the specific parameters for Ru_xS_y (sulfur-passivated Ru nanoparticles) do not exist. Applying the models utilized for the Mo- and Rh-based electrocatalysts to the $Re_xRu_yS_z$ material did not provide a fit of adequate quality, and this is reflected by the unrealistically high E_0 values in Table 2.

3.2. RRDE

3.2.1. Voltammetry

Representative cyclic voltammograms (CVs) for the standard 30 wt% Pt/C and Rh_xS_y/C (De Nora/SF and NA) electrocatalysts in 0.5 M H_2SO_4 and 0.5/1.0 M H_2SO_4/methanol electrolytes are presented in Fig. 6. The Pt/C electrocatalyst exhibited the well-established cathodic and anodic features of H/H^+ and oxo-species adsorption/desorption in acid electrolyte. In the presence of 1 M methanol (current divided by a gross factor of five for ease of visual comparison) the massive cathodic and anodic peaks at >0.50 V are attributed to irreversible methanol oxidation. Both varieties of Rh_xS_y/C exhibited a large, shallow cathodic feature beginning at ~0.7 V, and did not exhibit an H desorption feature of any appreciable magnitude. In agreement with a recent report by Papageorgopoulos et al. [64] the balanced phase De Nora catalyst [28] showed unambiguous evidence of methanol oxidation at potentials >0.60 V, but the oxidation currents are considerably lower. This is most likely a result of the methanol concentration; their unique cell design operates in a 4.0-M methanol concentration whereas this study involved a significantly lower concentration (1 M methanol). In contrast to the De Nora catalyst, the NA material showed only a small change in the current above 0.70 V suggesting that the magnitude of methanol oxidation is negligible.

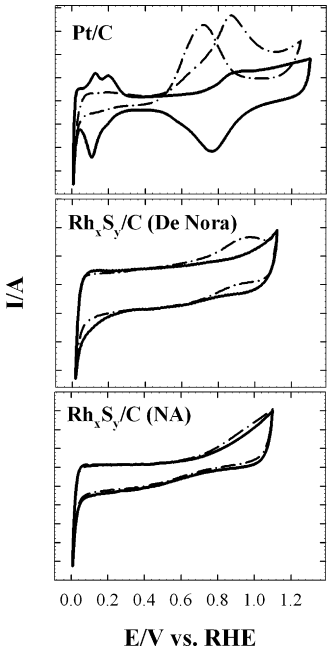

Fig. 6. Non-IR-corrected room temperature 20 mV s^{-1} cyclic voltammograms in de-aerated 0.5 M H_2SO_4 (solid line) and 0.5/1.0 M H_2SO_4/methanol (dashed line). For clarity, the magnitude of the current for Pt/C in methanol has been divided by five.

CVs of the Ru-based chalcogenides are presented in Fig. 7. In respect to the ternary compounds, no redox peaks from the incor-

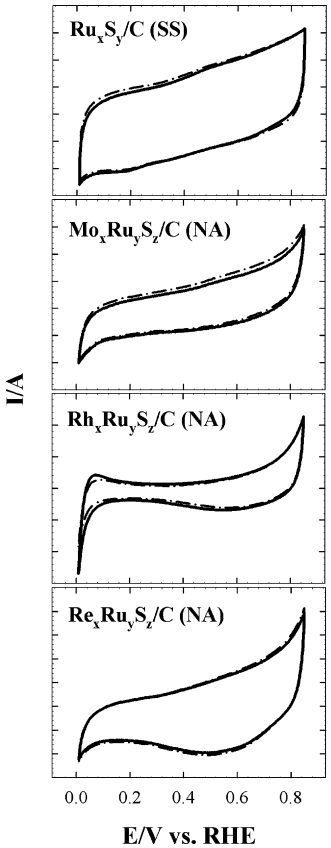

Fig. 7. Non-IR-corrected room temperature 20 mV s^{-1} cyclic voltammograms de-aerated 0.5 M H_2SO_4 (solid line) and 0.5/1.0 M H_2SO_4/methanol (dashed line).

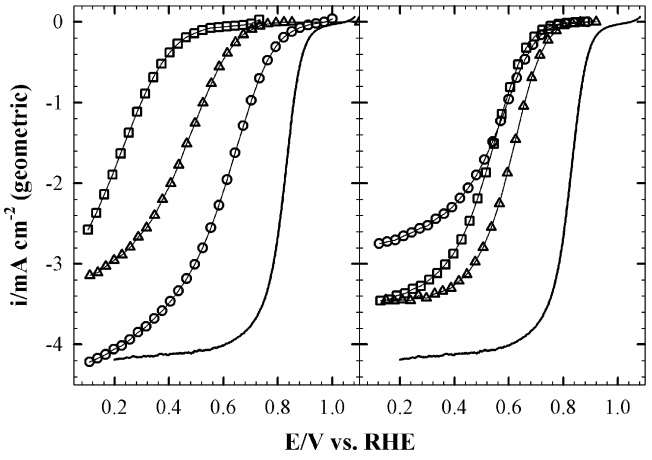

Fig. 8. 900 rpm ORR curves in room temperature O_2-saturated 0.5 M H_2SO_4 at 20 mV s^{-1}. Left: Pt (BASF, —), Rh_xS_y (De Nora/SF, ○), Rh_xS_y (NA, △), and Ru_xS_y (SS, □). Right: Pt (BASF, —), $Mo_xRu_yS_z$ (NA, ○), $Rh_xRu_yS_z$ (NA, △), and $Re_xRu_yS_z$ (NA, □).

porated transition metals were observed thus expressing the high quality of the synthetic procedures. Ru_xS_y/C (SS) (Fig. 7, top) shows slight cathodic and anodic features at 0.15 and 0.55 V, respectively, which did not appear in the NA-synthesized materials. The three $M_xRu_yS_z$/C (M = Mo, Rh, or Re) NA catalysts showed a broad cathodic feature down to E = 0.20 V, with the magnitude increasing in respect to the atomic number of the incorporated transition metal (i.e. Re > Rh > Mo). None of the materials exhibited a significant change in the CVs when methanol was added to the electrolyte.

3.2.2. ORR kinetics in 0.5 M H_2SO_4

Representative ORR curves (900 rpm, 20 mV s^{-1}) of the electrocatalysts in O_2-saturated 0.5M H_2SO_4 are presented in Fig. 8. It is immediately obvious that none of the materials are comparable to a state of the art Pt/C electrocatalyst in uncontaminated acid electrolyte (Table 3). Rh_xS_y/C (De Nora/SF) exhibited a high E_{onset} of 0.96 (compared to 1.02 V for Pt/C), where reduction currents started at 0.86 and 0.64 V for Rh_xS_y/C (NA) and Ru_xS_y/C (SS), respectively. In respect to E_{onset} (determined by a first derivative analysis of the ORR curves), the performance characteristics of the binary chalcogenides can be qualitatively assigned as Pt/C > Rh_xS_y/C (De Nora/SF) > Rh_xS_y/C (NA) > Ru_xS_y (SS). Akin to Rh_xS_y/C (NA), the Ru-based NA electrocatalysts (Fig. 8, right) reveal similar E_{onset} values of ~0.85 V with the exception of the Re-based material. Close inspection of this region indicates a qualitative performance trend of $Rh_xRu_yS_z$/C > $Mo_xRu_yS_z$/C > $Re_xRu_yS_z$/C (Table 3).

The kinetic current contributions in the ORR via RRDE can be quantitatively described through a series of relationships developed over the past several decades [1,65]. For a first order process [66], the overall current density (i) can be described from the contributions of the diffusion limited (i_{lim}) and kinetic (i_k) current densities:

$$\frac{1}{i} = \frac{1}{i_{lim}} + \frac{1}{i_k} \quad (1)$$

By determining i_{lim} the kinetic contribution can be extracted out of the overall current. An additional contribution to i_{lim} is composed of contributions from the diffusion-limited current density (i_d) and the transport through the Nafion® film/binder represented by "i_f":

$$\frac{1}{i_{lim}} = \frac{1}{i_d} + \frac{1}{i_f} \quad (2)$$

It has been demonstrated that by limiting the amount of Nafion® binder in the electrocatalyst ink, the contribution from i_f becomes negligible [6,50]. This is the case for our experimental processes (see Section 2.3) thus i_{lim} can be equated wholly to i_d. While the diffusion effects of the Nafion® binder can be neglected in our case, it should be noted that several of the chalcogenide electrocatalysts do not exhibit a smooth, flat i_{lim} (Fig. 5). Under these circumstances, the value for i_{lim} was designated as the point at which the slope of the mass-transfer controlled current became constant via a first derivative analysis of the ORR curve. The value for i_{lim} can be represented as

$$i_{lim} = B\omega^{1/2} \qquad (B = 0.62 n_e F A D^{2/3} \upsilon^{-1/6} C_{O_2}) \quad (3)$$

where ω is the angular rotation rate (radians s^{-1}), n_e is the number of electrons transferred, F is the Faraday constant, A is geometric electrode area (cm^2), D is the diffusion coefficient, υ is the kinematic viscosity, and C_{O_2} is the concentration of dissolved oxygen in the corresponding electrolyte [6]. When i_{lim} is the same as i_d, the mass transfer-corrected kinetic current (in the mixed kinetic-diffusion region) can be extracted from Eq. (1):

$$i_k = \frac{(i_{lim} \times i)}{(i_{lim} - i)} \quad (4)$$

Applying these relationships to the ORR curves, the corresponding Tafel plots in Fig. 9 are revealed. The standard Pt/C catalyst exhibits a kinetically controlled region from ~0.90–0.70 V, and exhibits two Tafel slopes of −55/126 mV dec^{-1}. The change in slopes is commonly attributed to inhibition of ORR through interference of OH_{ads} [32,67]. A slope of −120 mV dec^{-1} in the kinetically controlled region corresponds to a Tafel slope of $\sim -2 \times 2.3RT/F$ indicating a full $4e^-$ transfer (complete reduction of O_2 to H_2O) [32,50].

With the exception of Ru_xS_y/C (SS), the chalcogenide electrocatalysts show a similar range of kinetic current densities with Rh_xS_y/C (De Nora/SF) operating at a considerably lower overpotential. The NA materials are generally within a range of ~0.80–0.60 V, despite the chemical nature of the nanoparticle core. Rh is well known to possess a considerably higher activity for ORR than Ru in low pH environments [24,68]. However, in agreement with a recent report [24], sulfiding the Rh nanoparticles decreases performance. Despite operating at appreciably higher overpotentials, the chalcogenide electrocatalysts (outside of Ru_xS_y/C material) exhibit

Table 3
ORR kinetics determined in room temperature, O_2-saturated 0.5 M H_2SO_4 at 900 rpm and 20 mV s^{-1}

Catalyst (30 wt%)	E_{onset}[a] (V vs. RHE)	$-b$ (mV dec^{-1})	i_0 (mA cm^{-2})[b]	Maximum %H_2O_2	E at % H_2O_{2max} (V vs. RHE)
Pt/C (BASF)	1.02	56/126	1.8×10^{-4}	0.8	0.35
Rh_xS_y/C (SF)	0.96	52/122	7.8×10^{-5}	3.0	0.38
Rh_xS_y/C (NA)	0.85	59/111	1.6×10^{-7}	2.0	0.35
$Mo_xRu_yS_z$/C (NA)	0.86	109	2.5×10^{-7}	3.0	0.55
$Rh_xRu_yS_z$/C (NA)	0.88	112	5.6×10^{-7}	2.0	0.52
$Re_xRu_yS_z$/C (NA)	0.78	57/115	4.8×10^{-8}	3.5	0.30
Ru_xS_y/C (SS)	0.64	24/281	2.9×10^{-11}	10.0	0.35

[a] Determined by first derivative analysis of the ORR curve.
[b] Based on *geometric* surface areas.

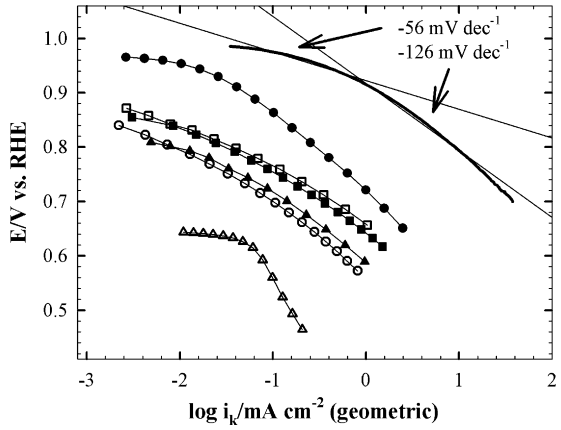

Fig. 9. Mass transfer-corrected Tafel plots for 900 rpm (20 mV s^{-1}) cathodic sweeps in room temperature O_2-saturated 0.5 M H_2SO_4: Pt (BASF, —), Rh_xS_y (De Nora/SF, ●), Rh_xS_y (NA, ○), $Mo_xRu_yS_z$ (NA, ■), $Rh_xRu_yS_z$ (NA, □), $Re_xRu_yS_z$ (NA, ▲), and Ru_xS_y (SS, △). Rotation rate: 900 rpm, scan rate: 20 mV s^{-1}.

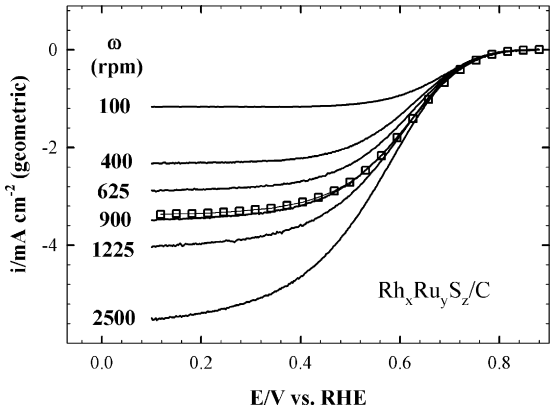

Fig. 10. Cathodic RDE curves for 30 wt% $Rh_xRu_yS_z$/C in 0.5 M H_2SO_4 (—) and comparison 900 rpm curve in 0.5/1.0 M H_2SO_4/methanol (□) under O_2-saturated, room temperature conditions.

~−60/120 mV dec^{-1} Tafel slopes (Table 3) similar to Pt/C. One interesting aspect is the considerably muted 60/120 mV dec^{-1} Tafel slope "switch" observed for the NA-synthesized materials with the −120 mV dec^{-1} region dominating the signals. Considering the low peroxide yields of these materials (Table 3), the ORR pathway and mechanism can be considered to be approximately identical as Pt (i.e. $\alpha = 0.5$, $n_e = 4$). Therefore, based on previous water activation studies conducted of state of the art Pt electrocatalysts [6,69], this observation suggests that the NA-synthesized materials are less predisposed towards OH_{ads}. The most likely cause would be inhibition due to the presence of sulfur on the catalyst surface. Whether or not this arises from bifunctional or electronic effects [5,6,69,70] is unclear from these studies, and is worthy of future investigation.

The Ru_xS_y/C (SS) catalyst represents the lowest-performing catalyst ($\eta \approx 600$ mV). In addition, the derived Tafel slopes (−24/281 mV dec^{-1}) defies any clear interpretation in respect to the generally accepted models previously outlined. There are several likely causes for this. First, while an approximation of i_{lim} can be discerned for the other chalcogenides, the Ru_xS_y/C (SS) does not display a limiting current (Fig. 8). Because i_{lim} could not be adequately assigned, a mass transfer correction could not be applied to the Tafel slope in Fig. 9. As a result, the Tafel parameters should be taken only as a very general approximation. Further, even if the Tafel plot represents the true mass transfer-corrected i_k for the Ru_xS_y/C (SS) electrocatalyst, the possibility of a deviation from $\alpha = 0.5$ should to be considered. Studies on $Mo_xRu_ySe_z$/C [54] and Ru_x/C [71] suggest that the α-value for nonaqueous-synthesized Ru-based electrocatalysts is appreciably greater than 0.5. In a previous study regarding oxygen depolarized cathodes (ODCs) for electrolytic chlorine generation cells (ORR in ≥0.5 M hydrochloric acid at 80 °C) [30] the Ru_xS_y/C (SS) system was found to be extremely stable when compared to NA-synthesized analogues when operated in the cell (~5 M HCl electrolyte), but the NA-synthesized Ru_xS_y/C materials were the performance leaders in the RDE experiments (O_2-saturated 0.5 M HCl). However, ODCs function as the counter electrodes in these systems, and operate within a potential window of 0.6–0.4 V [30,72,73]. Thus, while the Ru_xS_y/C (SS) is indisputably stable when operating as a "sink" (counter electrode) in extremely corrosive environments, the increased stability resulting from the SS-synthesis results in a loss of activity too great for effective employment as a cathode in PEM fuel cell applications.

In agreement with the XAS results (Section 3.1.2), and well-established examples in the literature [11,15,16,24], the ORR performance of the NA materials was not affected by the addition of 1 M methanol. For brevity, a full discussion of these results will not be presented beyond a representative graph of the $Rh_xRu_yS_z$/C electrocatalyst (Fig. 10). Further, while a complete discussion of the ORR performance of the De Nora Rh_xS_y/C electrocatalyst in methanol-containing acid electrolyte is warranted, the considerable complexity of this balanced phase (Rh_2S_3, Rh_3S_4, and $Rh_{17}S_{15}$) material [28,29] requires a separate publication. At the present time a detailed *in situ* XAS and electrochemical analysis being conducted [61], but the results are not yet mature enough for release.

3.2.3. Activation energies

Activation energies were derived from RDE data with an Arrhenius-type equation according to prior reports: [50]

$$\left(\frac{\delta \log(i_k)}{\delta(1/T)}\right)_E = \frac{E_a^*}{2.3R} \quad (5)$$

where T is the temperature (K), R the gas constant, and E represents the electrochemical potential within the envelope of high Tafel slope (e.g. ~120 mV dec^{-1}) before the effects of mass transport become apparent. The results of this analysis are presented in Fig. 11. Unfortunately, owing to both the wide temperature ranges and necessary time frame for data collection, the Rh_xS_y/C (NA) and Ru_xS_y/C (SS) electrocatalysts were too unstable to be reliably evaluated, and therefore these specific materials are immediately ruled out as viable electrocatalysts for fuel cell applications. This

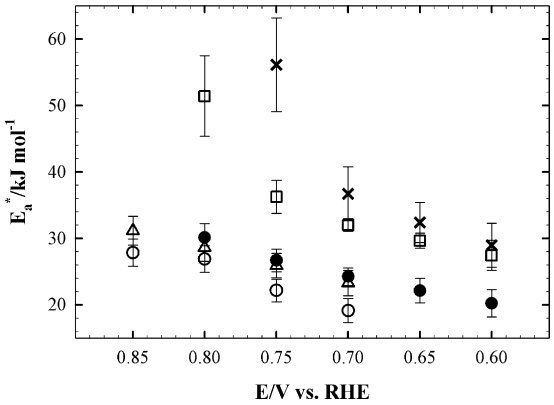

Fig. 11. Determined E_a^* values in O_2-saturated 0.5 M H_2SO_4 (900 rpm rotation rate) for: Pt/C (E-TEK, ○), Rh_xS_y/C (De Nora/SF, △), $Mo_xRu_yS_z$/C (□), $Rh_xRu_yS_z$/C (●), and $Re_xRu_yS_z$/C (×). The evaluation of the Pt/C electrocatalyst was performed in 1 M TFMSA (see Ref. [6]).

Table 4
Activation Energies (900 rpm, 0.5 M H_2SO_4)

Catalyst	E_a^* (kJ mol^{-1})						$E_{a\ \eta=0}^*$ [c] (kJ mol^{-1})
	0.85 V	0.80 V	0.75 V	0.70 V	0.65 V	0.60 V	
Pt/C[a]	27.84 ± 2.04	26.87 ± 2.0	22.13 ± 1.7	19.12 ± 1.8	N/A	N/A	52
Rh_xS_y/C[b]	31.14 ± 2.15	28.58 ± 2.05	25.90 ± 1.82	23.26 ± 1.9	N/A	N/A	51
$Mo_xRu_yS_z$/C	N/A	51.41 ± 6.05	36.25 ± 2.5	32.01 ± 0.95	29.64 ± 1.16	27.43 ± 2.28	63
$Rh_xRu_yS_z$/C	N/A	30.12 ± 2.12	26.67 ± 1.7	24.23 ± 1.33	22.12 ± 1.86	20.19 ± 2.04	51
$Re_xRu_yS_z$/C	N/A	N/A	56.14 ± 7.04	36.70 ± 4.07	32.38 ± 3.02	28.95 ± 3.3	78

[a] In 1 M trifluoromethanesulfonic acid (see Ref. [6]).
[b] Commercially available (SF) De Nora catalyst. Originally reported in Ref. [28].
[c] Extrapolated from a linear regression (Fig. 11).

was almost the case for the $Re_xRu_yS_z$/C material as reflected by the considerably large error bars (Fig. 11).

The determined E_a^* values of the catalysts trend downward in respect to increasing overpotential. Without exception, the magnitudes of the chalcogenide E_a^* values, at any given potential, are higher than the standard Pt/C electrocatalyst. Based on the prior electrochemical analysis, it is reasonable that the Pt/C catalyst would exhibit a lower activation barrier based on the exhibited superior performance. Activation energies have been reported for Pt/C [6,50] and Pt–M/C (M = Co, Fe, or Mo) [6,69] electrocatalysts via RDE experiments with the overall results summarized in recent report by Neyerlin et al. [74] In light of these observations, it is therefore unsurprising that the Rh_xS_y/C (De Nora/SF) and $Rh_xRu_yS_z$/C (NA) catalysts possess considerably lower E_a^* values than the Mo/Re-ternary analogues.

Considering the first electron transfer to be the rate-determining step for ORR, this trend was described [57,75] to relate to differences in oxide layer formation appearing in the pre-exponential factor of the Arrehnius equation due to a surface coverage effect:

$$i = n_e FkC_{O_2}(1 - \Theta_{ads}) \exp\left(\frac{-\beta FE}{RT}\right) \exp\left(\frac{-\gamma r_{\Theta_{ads}}}{RT}\right) \quad (6)$$

where k is the rate constant, Θ_{ads} is the surface coverage of adsorbed intermediates, E is the applied potential, β and γ represent the symmetry factors, $r_{\Theta ads}$ is the apparent ΔG of adsorption of the oxide layer, and all other variables have their standard meanings. Thus the coverage of Ru nanoparticles with sulfur increases the ORR activity of the electrocatalysts, and gives an E_a^* trend analogous to Pt/C. With the exception of Ru_xS_y/C (SS), the chalcogenide catalysts all exhibited a Tafel slope of ~120 mV dec^{-1} indicating a kinetic ORR pathway similar to Pt/C where the initial charge transfer is the rate-determining step.

As correlated with the SEM and XAS analysis, the additional of transition metals increases the activity of Ru_xS_y/C (NA). In the non-aqueous synthetic procedure, incorporation of $Mo(CO)_x$ or $Rh(CO)_x$ to the $Ru(CO)_x$/xylenes mixture increases the ORR activity of the final electrocatalyst with $Rh(CO)_x$ resulting in the highest performance. In comparison, the $Re_xRu_yS_z$ material should be considered as a mixture of Ru_xS_y/C (NA) and RuO_2 based on the *in situ* XAS results. As deduced from the XAS analysis Ru–M (M = Mo, Rh, or Re) interactions are not present. Instead, as Rh is inherently more stable than Mo in low pH environments [68], it would appear that the resulting propensity of M oxide formations serves as a buffer to oxidation/corrosion of the Ru nanoparticles. The Re additive is excessively oxidized in a comparatively short time [68,76], and quickly peters out as an effective ORR electrocatalyst. These results suggest that adding Mo or Rh improves the performance of Ru_xS_y/C (NA) in terms of a physical-mixing effect, and not as a chemical/electronic effect. In contrast to prior reports [15], adding Re to the synthesis results in a comparatively unstable mixture of RuO_2/Ru_xS_y resulting in considerably lower performance, activity, and stability.

Interpolation of the E_a^* slopes (Fig. 11) to $\eta = 0$ results in the energy values presented in Table 4. The reported $E_{a\ \eta=0}^*$ values for Pt vary over a considerable range, but are generally accepted to be ~60 kJ mol^{-1}. The extrapolated values for the highest performing electrocatalysts in this study (Pt/C, Rh_xS_y (De Nora/SF), and $Rh_xRu_yS_z$/C) are 51 kJ mol^{-1}. In contrast, the $Mo_xRu_yS_z$/C and $Re_xRu_yS_z$/C catalysts exhibit much higher energies of 63 and 78 kJ mol^{-1}, respectively. Considering that the E_a^* values are fundamentally influenced by the nature of the electrocatalyst surface [57,75], this suggests that the Mo/Re-ternary electrocatalysts are significantly different than $Rh_xRu_yS_z$/C. It has already been shown that the Mo and Re to Ru atomic ratios are considerably smaller than Rh:Ru (Table 1). In addition, the preceding XAS analysis of the $Re_xRu_yS_z$/C electrocatalyst has shown that it is most likely a mixture of carbon-supported Ru_xS_y and RuO_2 nanoparticles. Coupled with the determined activation energies, this suggests that although the transition metals are not incorporated into the Ru_xS_y/C matrix, their addition and eventual dissolution results in a change of the surface structure. Thus while the overall kinetic pathway for ORR is similar to Pt/C, the actual surface sites for the reactions on the chalcogenide materials are unique. Efforts to elucidate these surfaces *in situ* (akin to our prior study with the De Nora Rh_xS_y/C electrocatalyst) [28] are now underway, and are anticipated to provide similarly detailed information.

4. Conclusions

Ru- and Rh-based sulfide chalcogenide electrocatalysts were studied with a variety of electrochemical and morphological characterization techniques to provide insight into the structure/property relationships of these materials for ORR. The commercially available Rh_xS_y/C (De Nora) electrocatalyst, composed of three distinct Rh–S phases, noticeably outperformed the materials synthesized via the "nonaqueous" method; including an Rh_xS_y/C analogue by a wide margin. The nonaqueous electrocatalysts were comprised of metal nanoparticles passivated by an undetermined amount of sulfur. For the ternary compounds $M_xRu_yS_z$/C (M = Mo, Rh, or Re), it was discovered that the active portions of the Mo- and Rh-based materials was Ru_xS_y. For all three ternaries, XAS analysis showed no evidence of M–Ru interactions. In contrast to the Mo- and Rh-based systems, the $Re_xRu_yS_z$ electrocatalyst was comprised of RuO_2 and sulfur-passivated Ru nanoparticles resulting in poor ORR performance. The Ru_xS_y/C electrocatalyst, synthesized via a high temperature disproportionation route, while providing a degree of long-range order and stability exhibited by the De Nora Rh_xS_y/C electrocatalyst, had the lowest activity for ORR of all the electrocatalysts. Measured activation energies suggested a trend in accordance with the determined kinetic parameters, and showed that the Rh_xS_y/C (De Nora/SF) and $Rh_xRu_yS_z$/C (nonaqueous) electrocatalysts possess activation energies at $\eta = 0$ similar to Pt. These results indicate that these

chalcogenides conduct ORR in a mechanism similar to Pt arising from an availability of chemically analogous reaction sites. Owing to the superior stability and performance of the De Nora Rh_xS_y/C electrocatalyst over the other chalcogenides, it is apparent that the nonaqueous synthesis does not result in materials of adequate stability and activity, and it is therefore important to investigate new synthetic methodologies to create electrocatalysts capable of challenging state of the art Pt/C electrocatalysts for ORR application.

Acknowledgements

Financial and intellectual support was provided by the De Nora R&D Division, in particular Robert J. Allen, and is registered with the Office of Patents and Trademarks under the following numbers; US 6,967,185, US 6,149,782 and U.S. 6,358,381. Additional support was provided from the Army Research Office under a Multi-University Research Initiative (MURI) administered by Case Western Reserve University as P.I. Dr. Wen Wen (Chemistry Department, Brookhaven National Labs) assisted in the collection of the X-ray diffraction data at the National Synchrotron Light Source (beamline X-7B). Use of the National Synchrotron Light Source (beamlines X-7B, X-11A, and X-18B), Brookhaven National Laboratory, was supported by the U.S. Department of Energy, Office of Science, Office of Basic Energy Sciences, under Contract No. DE-AC02-98CH10886.

References

[1] A. Damjanovic, V. Brusic, Electrochim. Acta 12 (1967) 615.
[2] A. Damjanovic, M.A. Grenshaw, J.O.M. Bockris, J. Phys. Chem. 70 (1966) 3761.
[3] J. Lipkowski, P.N. Ross (Eds.), Electrocatalysis, Wiley-VCH, New York, 1998, p. 376.
[4] A. Wieckowski, E.R. Savinova, C.G. Vayanes (Eds.), Catalysis and Electrocatalysis at Nanoparticle Surfaces, Marcel Dekker, New York, 2003, p. 970.
[5] S. Mukerjee, R.C. Urian, Electrochim. Acta 47 (2002) 3219.
[6] V.S. Murthi, R.C. Urian, S. Mukerjee, J. Phys. Chem. B 108 (2004) 11011.
[7] M. Teliska, V.S. Murthi, S. Mukerjee, D.E. Ramaker, J. Electrochem. Soc. 152 (2005) A1259.
[8] Johnson-Matthey, The Platinum Metals Report: February 2007 Price Report, http://www.platinum.matthey.com/uploaded_files/pricereport0207.pdf, April 7, 2007.
[9] B. Wang, J. Power Sources 152 (2005) 1.
[10] A.K. Shukla, R.K. Raman, Annu. Rev. Mater. Res. 33 (2003) 155.
[11] N. Alonso-Vante, in: A. Wieckowski, E.R. Savinova, C.G. Vayenas (Eds.), Catalysis and Electrocatalysis at Nanoparticle Surfaces, Marcel Dekker, New York, 2003, p. 931.
[12] A.N. Vante, H. Tributsch, Nature 323 (1986) 431.
[13] N. Alonso Vante, B. Schubert, H. Tributsch, A. Perrin, J. Catal. 112 (1988) 384.
[14] N.A. Vante, W. Jaegermann, H. Tributsch, W. Hoenle, K. Yvon, J. Am. Chem. Soc. 109 (1987) 3251.
[15] R.W. Reeve, P.A. Christensen, A.J. Dickinson, A. Hamnett, K. Scott, Electrochim. Acta 45 (2000) 4237.
[16] R.W. Reeve, P.A. Christensen, A. Hamnett, S.A. Haydock, S.C. Roy, J. Electrochem. Soc. 145 (1998) 3463.
[17] V. Trapp, P. Christensen, A. Hamnett, J. Chem. Soc., Faraday Trans. 92 (1996) 4311.
[18] F. Dassenoy, W. Vogel, N. Alonso-Vante, J. Phys. Chem. B 106 (2002) 12152.
[19] N. Alonso-Vante, P. Borthen, M. Fieber-Erdmann, H.H. Strehblow, E. Holub-Krappe, Electrochim. Acta 45 (2000) 4227.
[20] N. Alonso-Vante, M. Fieber-Erdmann, H. Rossner, E. Holub-Krappe, C. Giorgetti, A. Tadjeddine, E. Dartyge, A. Fontaine, R. Frahm, J. Phys. IV 7 (1997) 887.
[21] I.V. Malakhov, S.G. Nikitenko, E.R. Savinova, D.I. Kochubey, N. Alonso-Vante, J. Phys. Chem. B 106 (2002) 1670.
[22] I.V. Malakhov, S.G. Nikitenko, E.R. Savinova, D.I. Kochubey, N. Alonso-Vante, Nuc. Instrum. Methods Phys. Res., Sect. A 448 (2000) 323.
[23] O. Solorza-Feria, K. Ellmer, M. Giersig, N. Alonso-Vante, Electrochim. Acta 39 (1994) 1647.
[24] D. Cao, A. Wieckowski, J. Inukai, N. Alonso-Vante, J. Electrochem. Soc. 153 (2006) A869.
[25] H. Schulenburg, M. Hilgendorff, I. Dorbandt, J. Radnick, P. Bogdanoff, S. Fiechter, M. Bron, H. Tributsch, J. Power Sources 155 (2005) 47.
[26] R.J. Allen, J.R. Giallombardo, D. Czerwiec, E.S. De Castro, K. Shaikh, De Nora S.p.A. (IT), US 6,358,381 (2002).
[27] J. Beck, T. Hilbert, Z. Anorg. Allg. Chem. 626 (2000) 72.
[28] J.M. Ziegelbauer, D. Gatewood, A.F. Gullá, D.E. Ramaker, S. Mukerjee, Electrochem. Solid-State Lett. 9 (2006) A430.
[29] J.M. Ziegelbauer, D. Gatewood, D.E. Ramaker, S. Mukerjee, ECS Trans. 1 (2005) 119.
[30] J.M. Ziegelbauer, A.F. Gullá, C. O'Laoire, C. Urgeghe, R.J. Allen, S. Mukerjee, Electrochim. Acta 52 (2007) 6282.
[31] A.F. Gullá, L. Gancs, R.J. Allen, S. Mukerjee, Appl. Catal. A: Gen. 326 (2007) 227.
[32] N.M. Marković, P.N. Ross, Surf. Sci. Rep. 45 (2002) 117.
[33] S. Mukerjee, in: A. Wieckowski, E.R. Savinova, C.G. Vayenas (Eds.), Catalysis and Electrocatalysis at Nanoparticle Surfaces, Marcel Dekker, New York, 2003, p. 501.
[34] Y.Y. Tong, A. Wieckowski, E. Oldfield, J. Phys. Chem. C 106 (2002) 2434.
[35] Q. Fan, C. Pu, K.L. Ley, E.S. Smotkin, J. Electrochem. Soc. 143 (1996) L21.
[36] Q. Fan, C. Pu, E.S. Smotkin, J. Electrochem. Soc. 143 (1996) 3053.
[37] C.A. Lucas, N.M. Marković, P.N. Ross, Phys. Rev. B 55 (1997) 7964.
[38] J.B.R. Rauhe, F. McLarnon, E.J. Cairns, J. Electrochem. Soc. 142 (1995) 1073.
[39] I. Villegas, M.J. Weaver, J. Chem. Phys. 101 (1994) 1648.
[40] N.S. Marinkovic, M.B. Vukmirovic, R.R. Adžić, in: R.E. White, B.E. Conway, C.G. Vayenas (Eds.), Modern Aspects of Electrochemistry, vol. 43, Springer, New York, 2007, p. 1.
[41] M. Hourani, A. Weickow-ski, J. Electroanal. Chem. 244 (1988) 147.
[42] C.K. Rhee, M. Wasberg, G. Horanyi, A. Wieckowski, J. Electroanal. Chem. 291 (1990) 281.
[43] R.J. Allen, A.F. Gullá, De Nora Elettrodi S.p.A. (IT), US 6,967,185 (2005).
[44] J. McBreen, W.E. O'Grady, K.I. Pandya, R.W. Hoffman, D.E. Sayers, Langmuir 3 (1987) 428.
[45] M. Teliska, W.E. O'Grady, D.E. Ramaker, J. Phys. Chem. B 109 (2005) 8076.
[46] M.A. Enayetullah, Ph.D., Case Western Reserve University, 1986.
[47] M.A. Enayetullah, T.D. DeVilbiss, J.O.M. Bockris, J. Electrochem. Soc. 136 (1989) 3369.
[48] D.C. Koningsberger, B.L. Mojet, G.E. van Dorssen, D.E. Ramaker, Top. Catal. 10 (2000) 143.
[49] M. Newville, J. Synchrotron. Radiat. 8 (2001) 322.
[50] U.A. Paulus, T.J. Schmidt, H.A. Gasteiger, R.J. Behm, J. Electroanal. Chem. 495 (2001) 134.
[51] T.J. Schmidt, U.A. Paulus, H.A. Gasteiger, R.J. Behm, J. Electroanal. Chem. 508 (2001) 41.
[52] Y. Shingaya, M. Ito, J. Electroanal. Chem. 467 (1999) 299.
[53] A. Kolics, A. Wieckowski, J. Phys. Chem. B 105 (2001) 2588.
[54] N. Alonso-Vante, H. Tributsch, O. Solorza-Feria, Electrochim. Acta 40 (1995) 567.
[55] H. Tributsch, M. Bron, M. Hilgendorff, H. Schulenburg, I. Dorbandt, V. Eyert, P. Bogdanoff, S. Fiechter, J. Appl. Electrochem. 31 (2001) 739.
[56] R.H. Castellanos, A. Camperos, O. Solorza-Feria, Int. J. Hydrogen Energy 23 (1998) 1037.
[57] U.A. Paulus, A. Wokaun, G.G. Scherer, T.J. Schmidt, V. Stamenkovic, V. Radmilovic, N.M. Marković, P.N. Ross, J. Phys. Chem. B 106 (2002) 4181.
[58] T.J. Schmidt, U.A. Paulus, H.A. Gasteiger, N. Alonso-Vante, R.J. Behm, J. Electrochem. Soc. 147 (2000) 2620.
[59] N. Alonso-Vante, I.V. Malakhov, S.G. Nikitenko, E.R. Savinova, D.I. Kochubey, Electrochim. Acta 47 (2002) 3807.
[60] S.P. Cramer, T.K. Eccles, F.W. Kutzler, K.O. Hodgson, L.E. Mortenson, J. Am. Chem. Soc. 98 (1976) 1287.
[61] J.M. Ziegelbauer, D. Gatewood, M. Guinel, F. Ernst, A.F. Gullá, D.E. Ramaker, S. Mukerjee (in preparation).
[62] M.J. Fay, A. Proctor, D.P. Hoffman, M. Houalla, D.M. Hercules, Microchim. Acta 109 (1992) 281.
[63] S.R. Wasserman, P.G. Allen, D.K. Shuh, J.J. Bucher, N.M. Edelstein, J. Synchrotron Rad. 6 (1999) 284.
[64] D.C. Papageorgopoulos, F. Liu, O. Conrad, Electrochem. Acta 52 (2007) 4982.
[65] A.J. Bard, L.F. Faulkner, Electrochemical Methods: Fundamentals and Applications, 2nd ed., John Wiley & Sons, Inc., New York, 2000.
[66] P.N. Ross, P.C. Andricacos, J. Electroanal. Chem. Interfacial Electrochem. 154 (1983) 205.
[67] M.R. Tarasevich, V.S. Vilinskaya, Electrokhimiya 9 (1973) 96.
[68] M. Pourbaix, Atlas of Electrochemical Equilibria in Aqueous Solutions, 1st ed., Pergamon Press, London, 1966.
[69] A.B. Anderson, J. Roques, S. Mukerjee, V.S. Murthi, N.M. Markovic, V. Stamenkovic, J. Phys. Chem. B 109 (2005) 1198.
[70] A.B. Anderson, T.V. Albu, J. Electrochem. Soc. 147 (2000) 4229.
[71] S. Duron, R. Rivera-Noriega, P. Nkeng, G. Poillerat, O. Solorza-Feria, J. Electroanal. Chem. 566 (2004) 281.
[72] F. Gestermann, Electrolysis in the Chemical Industry, Clearwater Beach, FL, 1998.
[73] F. Gestermann, A. Ottaviani, Modern Chlor-Alkali Technology, London 2001, SCI, London.
[74] K.C. Neyerlin, W. Gu, J. Jorne, H.A. Gasteiger, J. Electrochem. Soc. 153 (2006) A1955.
[75] N.M. Marković, H.A. Gasteiger, B.N. Grgur, P.N. Ross, J. Electroanal. Chem. 467 (1999) 157.
[76] V.O. Lavrenko, Zh. Fiz. Khim. (Rus. J. Phys. Chem.) 35 (1961) 1935.